JCI insight

Human antigen R as a therapeutic target in pathological cardiac hypertrophy

Lisa C. Green, … , Joshua B. Benoit, Michael Tranter

JCI Insight. 2019;4(4):e121541. https://doi.org/10.1172/jci.insight.121541.

Research Article | Cardiology | Cell biology

RNA binding proteins represent an emerging class of proteins with a role in cardiac dysfunction. We show that activation of the RNA binding protein human antigen R (HuR) is increased in the failing human heart. To determine the functional role of HuR in pathological cardiac hypertrophy, we created an inducible cardiomyocyte-specific HuR-deletion mouse and showed that HuR deletion reduces left ventricular hypertrophy, dilation, and fibrosis while preserving cardiac function in a transverse aortic constriction (TAC) model of pressure overload–induced hypertrophy. Assessment of HuR-dependent changes in global gene expression suggests that the mechanistic basis for this protection occurs through a reduction in fibrotic signaling, specifically through a reduction in TGF-β (*Tgfb*) expression. Finally, pharmacological inhibition of HuR at a clinically relevant time point following the initial development of pathological hypertrophy after TAC also yielded a significant reduction in pathological progression, as marked by a reduction in hypertrophy, dilation, and fibrosis and preserved function. In summary, this study demonstrates a functional role for HuR in the progression of pressure overload–induced cardiac hypertrophy and establishes HuR inhibition as a viable therapeutic approach for pathological cardiac hypertrophy and heart failure.

JCI insight

RESEARCH ARTICLE

Human antigen R as a therapeutic target in pathological cardiac hypertrophy

Lisa C. Green,[1,2] Sarah R. Anthony,[1] Samuel Slone,[1,2] Lindsey Lanzillotta,[1] Michelle L. Nieman,[2] Xiaoqing Wu,[3] Nathan Robbins,[1] Shannon M. Jones,[1] Sudeshna Roy,[4] A. Phillip Owens III,[1] Jeffrey Aube,[4] Liang Xu,[3] John N. Lorenz,[2] Burns C. Blaxall,[5] Jack Rubinstein,[1] Joshua B. Benoit,[6] and Michael Tranter[1]

[1]Department of Internal Medicine, Division of Cardiovascular Health and Disease and [2]Department of Pharmacology and Systems Physiology, University of Cincinnati College of Medicine, Cincinnati, Ohio, USA. [3]Department of Molecular Biosciences, University of Kansas, Lawrence, Kansas, USA. [4]Division of Chemical Biology and Medicinal Chemistry, Eshelman School of Pharmacy, University of North Carolina, Chapel Hill, North Carolina, USA. [5]Department of Pediatrics, Division of Molecular Cardiovascular Biology, Heart Institute, Cincinnati Children's Hospital Medical Center (CCHMC), Cincinnati, Ohio, USA. [6]Department of Biological Sciences, University of Cincinnati, Cincinnati, Ohio, USA.

RNA binding proteins represent an emerging class of proteins with a role in cardiac dysfunction. We show that activation of the RNA binding protein human antigen R (HuR) is increased in the failing human heart. To determine the functional role of HuR in pathological cardiac hypertrophy, we created an inducible cardiomyocyte-specific HuR-deletion mouse and showed that HuR deletion reduces left ventricular hypertrophy, dilation, and fibrosis while preserving cardiac function in a transverse aortic constriction (TAC) model of pressure overload–induced hypertrophy. Assessment of HuR-dependent changes in global gene expression suggests that the mechanistic basis for this protection occurs through a reduction in fibrotic signaling, specifically through a reduction in TGF-β (*Tgfb*) expression. Finally, pharmacological inhibition of HuR at a clinically relevant time point following the initial development of pathological hypertrophy after TAC also yielded a significant reduction in pathological progression, as marked by a reduction in hypertrophy, dilation, and fibrosis and preserved function. In summary, this study demonstrates a functional role for HuR in the progression of pressure overload–induced cardiac hypertrophy and establishes HuR inhibition as a viable therapeutic approach for pathological cardiac hypertrophy and heart failure.

Introduction

Heart failure (HF) is an increasing health burden that results from many common underlying factors, including hypertension, coronary artery disease, and myocardial infarction, and it is typically preceded by the enlargement, or hypertrophy, of the cardiac muscle — an effect that is initially beneficial and helps the heart maintain cardiac output in the face of hemodynamic stress (1). However, the development of left ventricular hypertrophy (LVH) in response to such a pathological stimulus is not sustainable and is associated with increased cardiac fibrosis, risk of arrhythmias, and development of HF. The current standard-of-care treatments for HF mostly aim to relieve the underlying pressure overload and/or reduce the workload on the heart through inhibition of overstimulated neurohumoral pathways (e.g., ACE inhibitors, angiotensin receptor blockers, diuretics, and β blockers) (2, 3). However, to our knowledge, no current therapies directly target the molecular signaling pathways in cardiac myocytes and fibroblasts that mediate LVH and fibrosis to prevent or reverse this pathological cardiac remodeling.

Human antigen R (HuR; encoded by the *Elavl1* gene) is an RNA binding protein that binds to AU-rich regions in the 3′-untranslated region of many different mRNAs, including many involved in inflammation, cell growth, and fibrosis, and it directly regulates the expression of target mRNA through modulation of its stability and/or translation (4, 5). While relatively little is known about the role of HuR in the myocardium, RNA binding proteins such as HuR are becoming recognized as potentially central regulators of cardiac physiology and pathology (6, 7). We have recently shown that HuR is both necessary and sufficient for hypertrophic growth in cultured primary rat myocytes in response to hypertrophic stimuli in vitro (8).

Authorship note: LCG and SRA contributed equally to this work.

Conflict of interest: The authors have declared that no conflict of interest exists.

Submitted: April 9, 2018
Accepted: January 14, 2019
Published: February 21, 2019

Reference information:
JCI Insight. 2019;4(4):e121541.
https://doi.org/10.1172/jci.insight.121541.

In this work, we show that HuR activation is increased in failing human hearts. We used a mouse model of transverse aortic constriction (TAC) to induce LV pressure overload, a well-established model of aortic stenosis, to demonstrate that cardiac myocyte–specific deletion of HuR protects against pathological remodeling and functional decline in this model. Importantly, we also utilize a potentially novel small molecular inhibitor of HuR to show that pharmacological inhibition of HuR at a clinically relevant time point following the onset of initial pathology improves survival and significantly slows the decline of cardiac function and progression of LV remodeling. Furthermore, HuR activity in the hypertrophic heart colocalizes with regions of fibrosis, and the development of fibrosis is blunted following either HuR deletion or pharmacological inhibition. Lastly, RNA sequencing (RNA-seq) analysis also suggests modulation of fibrotic signaling as a key mechanism to HuR-mediated cardiac pathology.

This work demonstrates a functional role for HuR in the development and progression of pathological LVH and HF. Importantly, we not only establish the benefit of HuR targeting using either inducible, tissue-specific HuR deletion or pharmacological inhibition, but we also begin to decipher the underlying mechanisms of this effect. Since, to our knowledge, there are currently no pharmacological inhibitors of HuR that have been demonstrated for in vivo applications, this work is also critical in demonstrating that HuR represents a viable therapeutic target for the treatment of pathological LVH and HF.

Results

HuR activation is increased in human HF. HuR resides predominately in the nucleus in an inactive form and translocates to the cytoplasm upon activation where it exerts its posttranscriptional regulation via target mRNA binding (4, 9). We have previously shown that HuR cytoplasmic translocation is increased in primary neonatal rat ventricular myocytes (NRVMs) following a hypertrophic stimulus (8). To determine HuR activity in failing human myocardium, we performed HuR immunofluorescence (IF) staining on both healthy donor hearts and tissue that was explanted during left ventricular assist device (LVAD) implantation. Representative images show an increase in HuR cytoplasmic translocation in failing human myocardium (LVAD) vs. healthy donor tissue (Figure 1). In addition, HuR staining also shows a similar pattern of increased HuR activation in a mouse model of TAC-induced pathological LVH (Supplemental Figure 1; supplemental material available online with this article; https://doi.org/10.1172/jci.insight.121541DS1).

Cardiac myocyte–specific deletion of HuR reduces development of pathological LVH. To achieve inducible cardiomyocyte-specific HuR deletion (*iCM-HuR*$^{-/-}$), we crossed HuR-floxed mice (*HuR*$^{fl/fl}$) (10) with mice expressing a cardiac myocyte–specific inducible Cre recombinase (*αMHC-mER-Cre-mER*) (11) and induced Cre recombinase activity through a daily i.p. injection of 4-hydroxy-tamoxifen (4-OHT) (60 mg/kg/day) for 5 days, as previously described (Supplemental Figure 2) (11). Importantly, deletion of HuR did not affect basal cardiac function (Supplemental Figure 3). The absence of a basal cardiac phenotype in *iCM-HuR*$^{-/-}$ mice is not surprising, given our data that HuR appears mostly inactive in adult myocardium under resting conditions (Figure 1 and Supplemental Figure 1).

To determine the role of HuR in pathological cardiac hypertrophy, *iCM-HuR*$^{-/-}$ mice and tamoxifen-treated *Cre*$^{+}$/*HuR*$^{+/+}$ littermate controls underwent TAC, a model of LV pressure overload that results in a predictable and reproducible progression from compensated LVH to decompensated LVH to HF. Sham procedure groups were included as surgical/manipulation control groups. At 8 weeks after TAC, *iCM-HuR*$^{-/-}$ hearts showed a preserved cardiac architecture and reduced hypertrophy (LV weight/body weight ratio) compared with *Cre*$^{+}$/*HuR*$^{+/+}$ control hearts (Figure 2, A and B). Interestingly, while myocyte-specific deletion of HuR did not completely inhibit the development of LVH, it did appear to completely inhibit the induced expression of the hypertrophic marker genes atrial natriuretic factor (ANF; *Nppa*) and brain natriuretic protein (BNP; *Nppb*) at 8 weeks following TAC (Figure 2, C and D).

HuR deletion delays the transition from compensated to decompensated LVH. Longitudinal assessment of LV mass (normalized to body weight) via echocardiography showed a significant increase in LV mass in control mice at 2 weeks following aortic constriction, whereas the LV mass of *iCM-HuR*$^{-/-}$ mice increased in a much more gradual manner (Figure 3A), with a significant blunting in total LV mass gain from baseline compared with control at 8 weeks after TAC (Figure 3B). Moreover, LV posterior wall thickness was significantly increased at 2 weeks after TAC in the control mice, followed by a gradual thinning of the LV wall, as expected, with a progression to decompensated hypertrophy and LV dilation (Figure 3C). However, much like the gradual progression of LV mass, the LV posterior wall thickness in *iCM-HuR*$^{-/-}$ mice showed a gradual hypertrophy, suggesting a delayed progression of the hypertrophic response in the absence of HuR (Figure 3C).

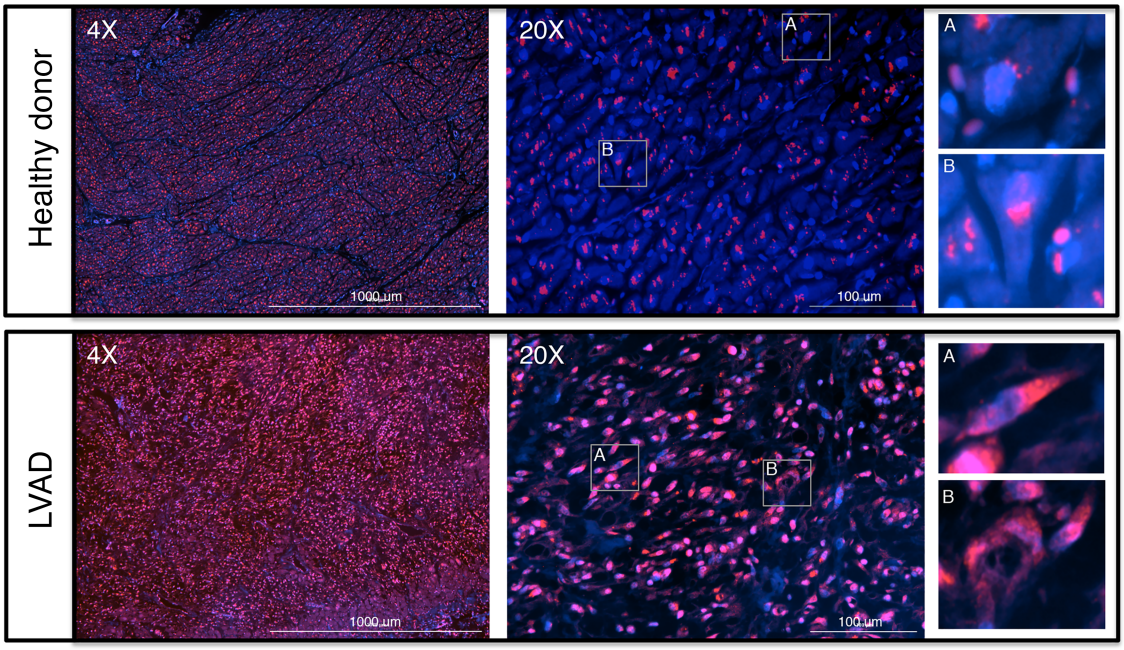

Figure 1. HuR activation is increased in failing human hearts. HuR immunofluorescence staining from healthy donor hearts, as well explanted tissue from left ventricular assist device (LVAD). HuR immunofluorescence staining from control sham and TAC mice. Scale bars: 1000 μm (4×), 100 μm (20×). Images are representative of n = 3/group.

LV dilation and wall thinning are both hallmarks of the maladaptive cardiac remodeling that occurs as pathological LVH progresses to decompensation and HF (12). Weekly assessment of both LV end diastolic (Figure 3D) and LV end systolic (Figure 3E) volume showed a significant reduction in LV dilation starting at 4 weeks after TAC in the *iCM-HuR*$^{-/-}$ mice. Accordingly, *iCM-HuR*$^{-/-}$ mice displayed significantly less LV dilation at 8 weeks after TAC than their littermate controls (Figure 3F).

HuR deletion preserves cardiac function following LV pressure overload. The initial development of hypertrophy is thought to be a compensatory response to maintain cardiac output in the face of hemodynamic stress. Because of this, there is concern by some that inhibition of the hypertrophic process may result in a rapid loss of systolic function in pressure overload. A modest decline in cardiac function, as measured via LV ejection fraction, was observed in both control and *iCM-HuR*$^{-/-}$ mice in the first few weeks following TAC (Figure 3G). However, as the control mice continued to decline from 6–8 weeks after TAC, LV ejection fraction in the *iCM-HuR*$^{-/-}$ mice remained stable and significantly improved compared with control (Figure 3G). At 8 weeks following TAC, total decline of LV ejection fraction was significantly less in the *iCM-HuR*$^{-/-}$ mice compared with control (Figure 3H).

In vivo, invasive pressure catheterization was performed to confirm equal pressure gradients between control and *iCM-HuR*$^{-/-}$ mice (Supplemental Figure 4) and to determine the rate of LV pressure changes in the 2 groups. Results show that *iCM-HuR*$^{-/-}$ mice had a preserved rate of both LV developed pressure (+dP/dt; Figure 3I) and LV relaxation (–dP/dt; Figure 3J).

Deletion of HuR reverses genome-wide changes in TAC-induced gene expression. To determine the mechanisms by which myocyte-specific HuR deletion mediates the hypertrophic response, we performed RNA-seq to identify HuR-dependent changes in transcript expression. RNA-seq was performed on control sham, *iCM-HuR*$^{-/-}$ sham, control TAC, and *iCM-HuR*$^{-/-}$ TAC hearts at 8 weeks following surgical manipulation (Figure 4A and Supplemental Table 1). Comparison of the sham groups confirmed that HuR played little role in mature, nonstressed myocytes, as HuR deletion had minimal impact on basal transcript levels; only 4 of 46,989 transcripts were found to be significantly dysregulated between control and *iCM-HuR*$^{-/-}$ sham groups (Supplemental Table 1). Applying a rather stringent statistical filter of a FDR at 0.01, we identified 2006 distinct mRNA transcripts whose expression was markedly altered by TAC (control sham vs. control TAC; Figure 4B and Supplemental Table 2). Applying the same strict statistical filter, we found that 59 of these genes were strongly regulated by HuR (Figure 4B, Supplemental Table 3, and Supplemental Table 6).

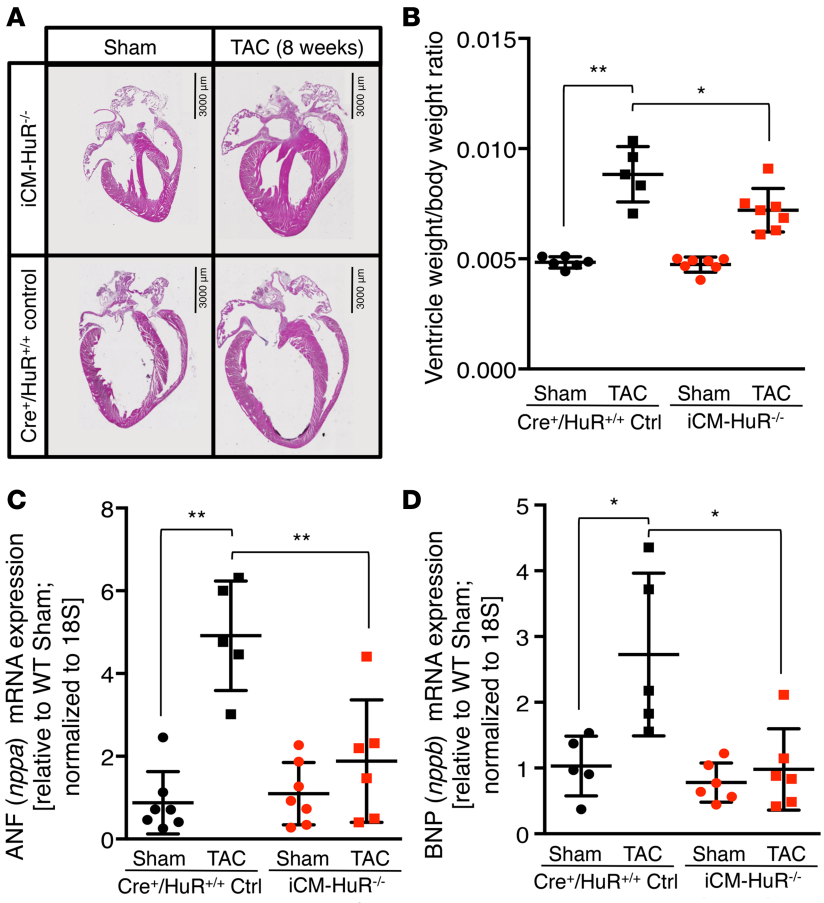

Figure 2. Cardiac-specific deletion of HuR reduces hypertrophy in response to TAC-induced LV pressure overload. (**A**) Hearts from control and iCM-HuR$^{-/-}$ mice were isolated 8 weeks after TAC or sham surgery. These hearts were then embedded in paraffin, sectioned, and H&E stained. Scale bar: 3000 μm. (**B**) Ventricular weight/body weight ratio of control and iCM-HuR$^{-/-}$ mice 8 weeks after TAC or sham surgery. qPCR for ANF (**C**) or BNP (**D**) mRNA levels from mice 8 weeks after sham or TAC surgery relative to 18S. For **B**–**D**, 2-way ANOVA was used to compare sham and TAC groups; *P <0.05 and **P <0.01 for indicated comparisons. Data are shown as means ± SEM. $n \geq 5$ per group.

Using a principal component analysis (PCA) plot to visualize broad-level changes in TAC and HuR-dependent changes in transcript expression showed the 2 sham groups clustering together with a strong shift in TAC-dependent transcript changes in control mice that was reversed in HuR-deletion mice (Figure 4C). A more in-depth look at the 2006 TAC-dependent transcript changes showed a recovery/reversal of TAC-induced changes in 1865 (92.9%) of these 2006 transcripts, with 1 (0.1%) being unaffected, and 140 (7.0%) being exacerbated upon HuR deletion (Figure 4D). Furthermore, all 59 of the transcripts identified as being strongly HuR dependent showed a reversal or recovery of TAC-mediated changes in *iCM-HuR*$^{-/-}$ mice (Figure 4D; inset).

Gene ontology (GO) clustering and enrichment analysis of the 59 HuR-dependent transcripts shows that HuR predominately regulated the expression of genes involved in cell growth and development (tissue development and system development) and fibrosis/ECM remodeling (fibril organization and collagen fibril organization) (Figure 4E). Given that pathological LVH is known to induce both cell growth (hypertrophy) and fibrotic signaling pathways, a reversal in the expression changes of these genes in *iCM-HuR*$^{-/-}$ mice is not unexpected (12).

HuR mediates the development of cardiac fibrosis. In accordance with the RNA-seq data suggesting a strong role for HuR in the development of cardiac fibrosis, we also observed a significant reduction in fibrosis in the *iCM-HuR*$^{-/-}$ hearts compared with control at 8 weeks after TAC (Figure 5). RNA-seq results show a significant HuR-dependent blunting of TAC-induced expression of 16 profibrotic genes (taken from the 59 identified HuR-dependent genes in Figure 4; Figure 6A). Furthermore, we show a robust increase in protein expression of periostin, a marker for activated myofibroblasts (13), in the control mice that was nearly ablated in the *iCM-HuR*$^{-/-}$ mice (Figure 6B).

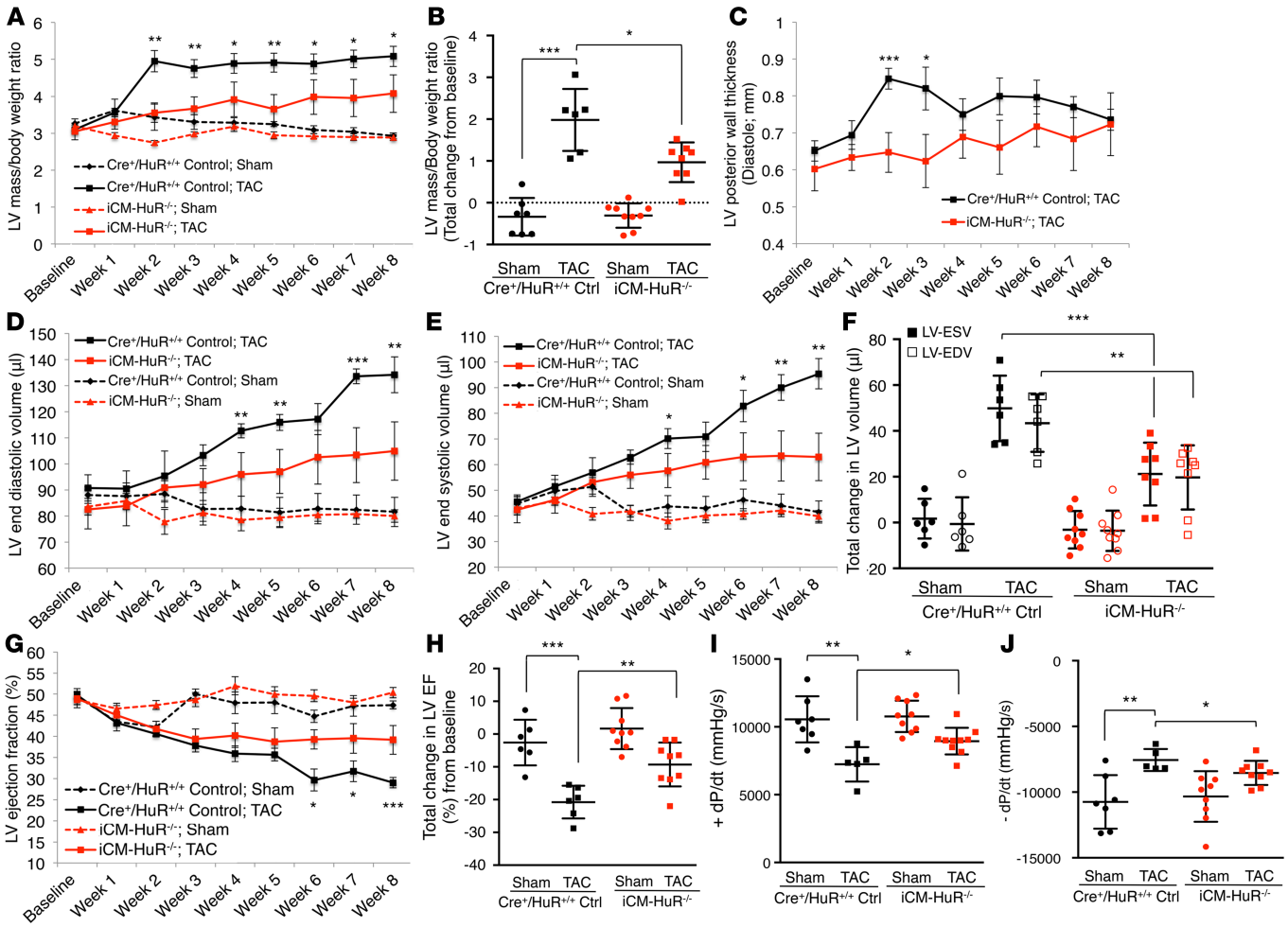

Figure 3. Cardiac-specific deletion of HuR delays progression from compensated to decompensated hypertrophy. (**A**) Left ventricular (LV) mass/body weight ratio of control and iCM-HuR$^{-/-}$ mice before TAC (baseline) and weekly until 8 weeks after TAC. (**B**) Quantification of the total LV mass/body weight ratio change from baseline to 8 weeks after TAC/sham surgeries. (**C**) LV posterior wall thickness, (**D**) LV end diastolic volume, and (**E**) LV end systolic volume quantified by echocardiography and baseline and weekly until 8 weeks after TAC or sham surgery. (**F**) Quantification of total LV end diastolic and systolic volume change from baseline to 8 weeks after TAC or sham surgeries. (**G**) LV ejection fraction of control and iCM-HuR$^{-/-}$ mice from baseline to 8 weeks after TAC or sham surgeries. (**H**) Quantification of total change in LV ejection fraction from baseline to 8 weeks after TAC or sham surgeries. (**I**) Positive and (**J**) negative ventricular contractility assessment (dP/dt) of control and iCM-HuR$^{-/-}$ mice 8 weeks after TAC or sham surgeries. For **A**–**H**, 2-way ANOVA and 2-tailed Student's *t* tests were performed. **P* <0.05, ***P* <0.01, and ****P* <0.001 for indicated comparisons. Data are shown as means ± SEM. $n \geq 6$ per group.

While compelling, this data alone does not allow us to conclude whether HuR deletion plays a direct role in the inhibition of fibrotic signaling in the heart or whether the reduction in fibrosis is an indirect consequence due to the inhibition of pathological LVH. However, activation of HuR in hypertrophic myocytes, at 8 weeks after TAC, colocalizes with regions of fibrosis (Figure 6C), supporting a functional link between the two. We utilized isolated NRVMs to show that *Tgfb* mRNA expression, in response to hypertrophic stimuli in cardiac myocytes, is dependent on HuR (Figure 6D). To demonstrate that HuR directly regulates *Tgfb* expression in myocytes, we performed an RNA-protein cross-linking immunoprecipitation (CLIP) to show direct binding of HuR to the *Tgfb* mRNA transcript (Figure 6E). Additionally, HuR appears to mediate *Tgfb* expression by stabilizing the transcript, as our results show that — following treatment with actinomycin D (2.5 µg/ml) — HuR inhibition led to expedited degradation of *Tgfb* mRNA (Figure 6F). Finally, a HuR-dependent role in *Tgfb* signaling in hypertrophy is also supported by our RNA-seq data showing a recovery of TAC-dependent gene expression changes for transcripts associated with positive regulation of *Tgfb* signaling (Figure 6G and Supplemental Table 4).

Pharmacological inhibition of HuR reduces further progression of LVH and preserves cardiac function. To determine the potential feasibility of inhibiting HuR as a therapeutic approach, we used KH-3, a potentially

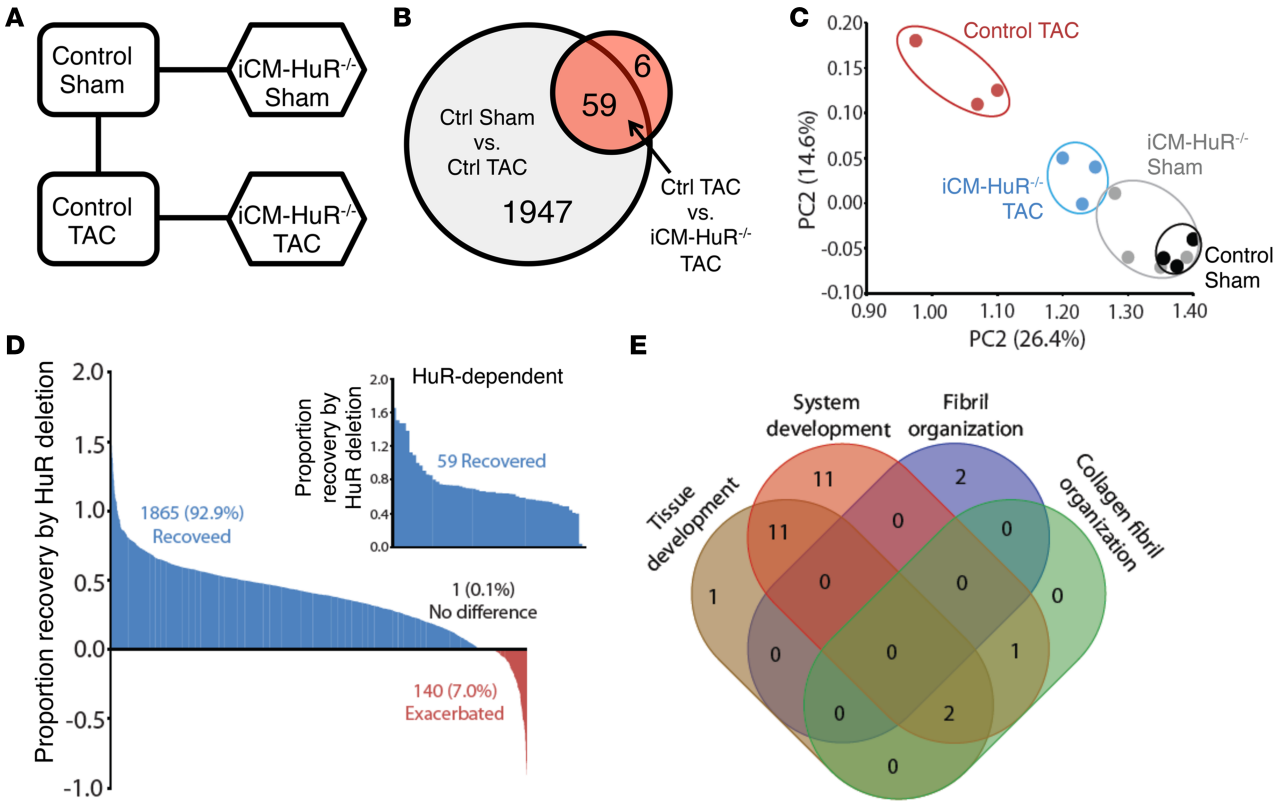

Figure 4. Identification of HuR-dependent changes in transcript levels. (**A**) Schematic for experimental groups compared, denoted by connecting line. (**B**) Venn diagram showing overlap in the number of transcripts with significant differences in control and iCM-HuR$^{-/-}$ mice following TAC. (**C**) Principal component (PC) analyses based on normalized expression values for RNA-seq data. (**D**) Proportion of expression change recovery in iCM-HuR$^{-/-}$ vs. control mice for all significant TAC-dependent gene expression changes (from Supplemental Table 1) between control sham and control TAC. Blue represents recovery following HuR deletion. Inset, overlapping set of significant HuR-dependent genes displayed in **B**. (**E**) Specific GO categories shifted during HuR dependent recovery that underlie changes in heart hypertrophy. $n \geq 3$ per group.

novel small-molecule inhibitor of HuR, to achieve in vivo inhibition following the initial onset of pathological LVH. We have previously demonstrated the inhibition of hypertrophic growth in vitro using earlier generation precursors of KH-3 (8). In this experiment, we subjected 20 mice to TAC and allowed them to progress for 4 weeks prior to randomization into 2 groups with indistinguishable cardiac mass and function (Supplemental Figure 5). These groups were then treated with either vehicle or KH-3 (60 mg/kg injected i.p. 3× weekly) for 7 additional weeks.

Mice treated with KH-3 displayed increased survival (Figure 7A) and maintained relatively normal sized hearts (Figure 7, B and C). Longitudinal assessment of LV mass confirmed that all animals had a significant increase in LV mass prior to initiating KH-3 treatment (Figure 7D). However, LV mass in vehicle treatment mice continued to increase, whereas KH-3 inhibited further increase in LV mass, and LV mass in KH-3 animals at 11 weeks after TAC was not significantly different than immediately prior to randomization (Figure 7, D and E). In addition, KH-3–treated animals had significantly less cardiac mass when normalized to either body weight or tibia length (Figure 7, F and G), as well as a significant reduction in ANF mRNA expression (Figure 7H). Treatment with KH-3 also significantly reduced further LV dilation (Figure 7, I and J).

KH-3 treatment was also able to significantly reduce the rate of decline in cardiac function. Echocardiography shows a significantly preserved LV ejection fraction in KH-3–treated mice compared with vehicle (Figure 7, K and L). KH-3 also showed a significant preservation in the rate of LV relaxation (–dP/dt) and a strong trend to preserving the rate of positive LV pressure generation (+dP/dt) (Figure 7, M and N). Importantly, we show via in vivo pressure catheterization that KH-3– and vehicle–treated groups had similar LV pressure gradients (Supplemental Figure 6) and that KH-3 treatment had no effect on peripheral blood pressure (Supplemental Figure 7 and Supplemental Figure 8).

Inhibition of HuR via KH-3 reduces cardiac fibrosis. Vehicle-treated hearts show a significant degree of cardiac fibrosis at 11 weeks after TAC (Figure 7O, upper panel), while treatment with KH-3 significantly

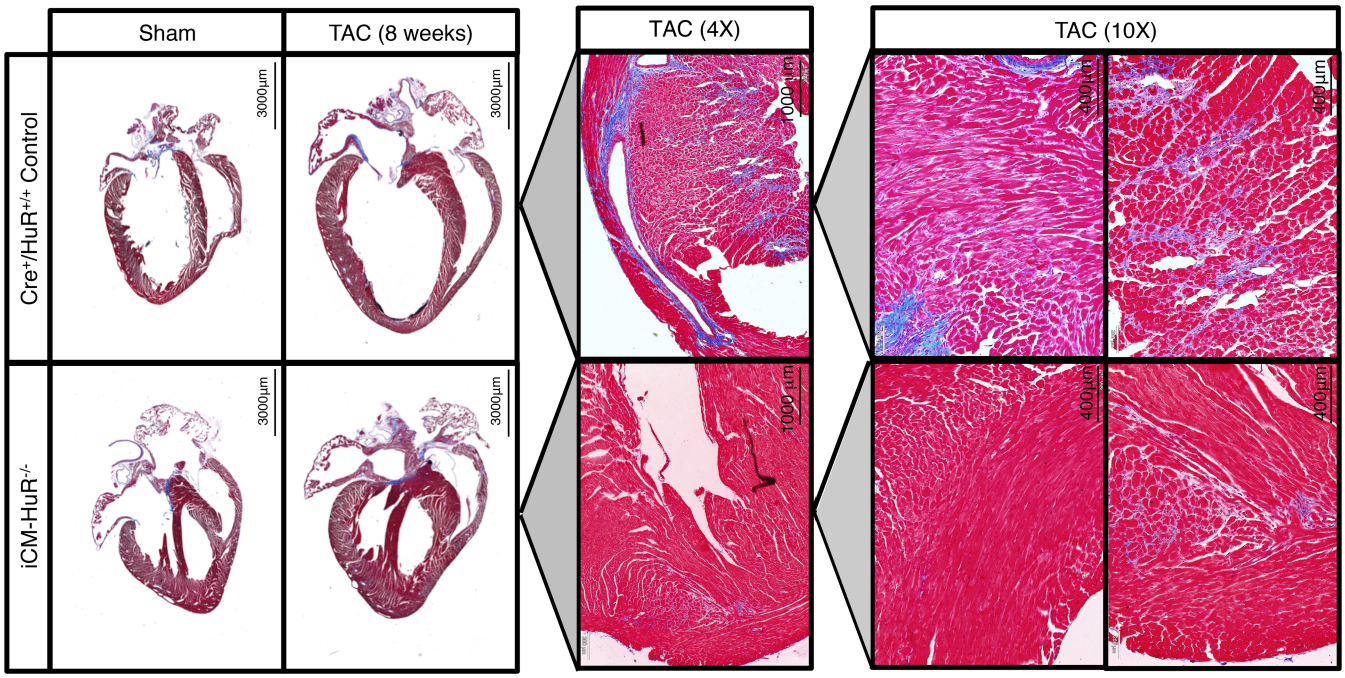

Figure 5. HuR blunts the development of cardiac fibrosis. Masson's trichrome images of sectioned hearts from control and iCM-HuR$^{-/-}$ mice after TAC or sham surgery. Scale bar: 3000 μm, 1000 μm, 400 μm (whole heart, 4×, and 10×).

reduced the amount of cardiac fibrosis (Figure 7O, lower panel). Interestingly, the overall reduction in fibrosis appears to be most strongly attributed to a reduction in interstitial fibrosis (Figure 7O, right panes). Western blotting also shows a significant reduction in the protein expression of fibronectin and periostin in mice given KH-3 (Figure 7P).

Discussion

Despite being highly expressed in the heart, relatively little is known about the role of HuR in the myocardium. However, there is growing interest in the functional role that HuR and other RNA binding proteins may play as central regulators of posttranscriptional gene expression in cardiac physiology and pathology (6, 7). To assess the functional role of HuR in the development and progression of pathological cardiac hypertrophy, we created the first cardiac-specific HuR deletion mouse to our knowledge (*iCM-HuR*$^{-/-}$). Characterization of these mice did not identify any basal differences in phenotype between *iCM-HuR*$^{-/-}$ and control mice, and HuR deletion had minimal impact on basal (sham) gene expression. This was expected, given our prior in vitro work (8), as well as results presented here, showing minimal cytoplasmic localization (activation) of HuR in nonstressed myocytes. However, following TAC, the *iCM-HuR*$^{-/-}$ mice were significantly protected from pathology, as evidenced by reduced LV hypertrophy, preserved cardiac function, reduced LV chamber dilation, and lessened cardiac fibrosis.

It is interesting to note that some degree of compensated LV hypertrophy still occurs in the *iCM-HuR*$^{-/-}$ mice. These results demonstrate that myocyte-specific deletion of HuR only partially blunts or slows the development of hypertrophy but more strongly reduces the pathological LV remodeling and fibrosis associated with progression to a decompensated phase and functional decline. It has been shown that load-induced compensated LV hypertrophy is not a strict requirement to maintain contractile performance in a mouse heart (14), and it has been argued that cardiac hypertrophy in response to pathological stimuli is not, in fact, a beneficial compensatory response (15). Thus, the protection observed from the deletion of HuR could be due to an inhibition of hypertrophic growth or to a more direct inhibition of 1 or more underlying mechanisms that drive the transition from a compensated hypertrophy to a state of pathological hypertrophy.

Prior work has suggested that HuR plays a central role in the cardiac response to stress following ischemia/reperfusion injury (myocardial infarction) (16, 17). Krishnamurthy, et al. show that HuR expression increases

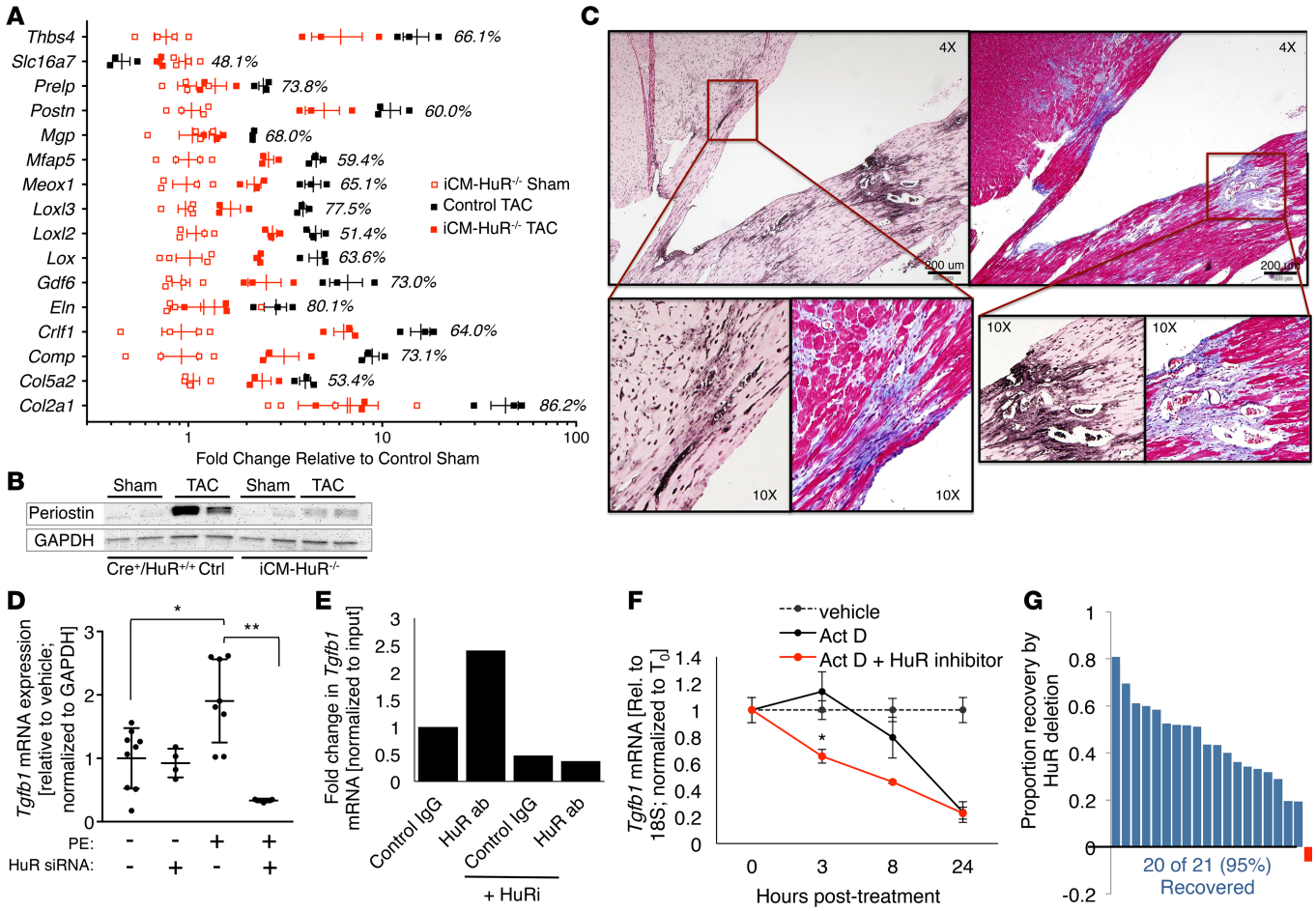

Figure 6. HuR mediates the development of cardiac fibrosis. (**A**) Expression of genes associated with tissue development/fibrosis that are differentially regulated in iCM-HuR$^{-/-}$ mice based on those identified in Figure 4E. Percent following bars in expressional recovery in iCM-HuR$^{-/-}$ compared with control during TAC. (**B**) Western blot for periostin protein expression from cardiac tissue isolated from control or iCM-HuR$^{-/-}$ mice 8 weeks after TAC or sham surgery. GAPDH protein expression serves as the loading control. (**C**) DAB staining of HuR (brown) alongside Masson's trichrome staining (blue indicative of fibrotic regions) of serial sections of the heart of a WT mouse 8 weeks after TAC. (**D**) TGF-β mRNA expression levels in response to a hypertrophic stimulus (Phenylepherine; PE) in the presence/absence of HuR determined by performing qPCR on RNA isolated from cultured neonatal rat ventricular myocytes with HuR siRNA/control siRNA; $n \geq 3$ replicates per treatment. (**E**) qPCR qualitative measure of *Tgfb* RNA eluted using a HuR antibody or a goat anti–rabbit IgG control in the presence and absence of a HuR inhibitor; representative $n = 1$. (**F**) qPCR quantification of *Tgfb* mRNA after treatment with vehicle, Actinomycin D (Act D), or Actinomycin D + HuR inhibitor; $n = 6$. (**G**) TAC-dependent transcripts associated with positive regulation of TGF-β (GO: 0071560) signaling based on Supplemental Table 2. Blue represents recovery following HuR deletion. For **D**, a 2-way ANOVA was performed. *P <0.05 and **P <0.01 for indicated comparisons. Data are shown as means ± SEM.

following ischemic injury and plays a role in mediating postinfarct remodeling and *Tgfb* expression. However, it was unclear from this work which cell types exhibited a central role for HuR, and the authors postulated a key role for HuR expression in infiltrating leukocytes. While HuR is certainly highly expressed in these cells, it is also expressed in many resident cell types within the myocardium, and our results are the first to our knowledge to demonstrate a clear role for HuR signaling specifically in myocytes. In this work, we show that HuR activation is increased in the myocytes of hypertrophic hearts and that the mechanistic basis of the protection observed in *iCM-HuR*$^{-/-}$ mice following TAC is potentially through an inhibition of *Tgfb* expression and subsequent development of cardiac fibrosis. This repressed level of *Tgfb* expression is confirmed in our RNA-seq studies, where additional positive regulators of this pathway were reduced and suppressive genes show little to no changes.

TGF-β is produced and secreted by myocytes in response to hypertrophic stimuli and can initiate myofibroblast activation (and subsequent cardiac fibrosis) in a paracrine fashion (18–20). TGF-β is increased in hypertrophic myocardium and is a primary initiator of myofibroblast activation and fibrotic signaling, which is a critical step that leads to extracellular matrix (ECM) remodeling and cardiac fibrosis (18, 19). However, the mechanistic details of how TGF-β expression is regulated in hypertrophic

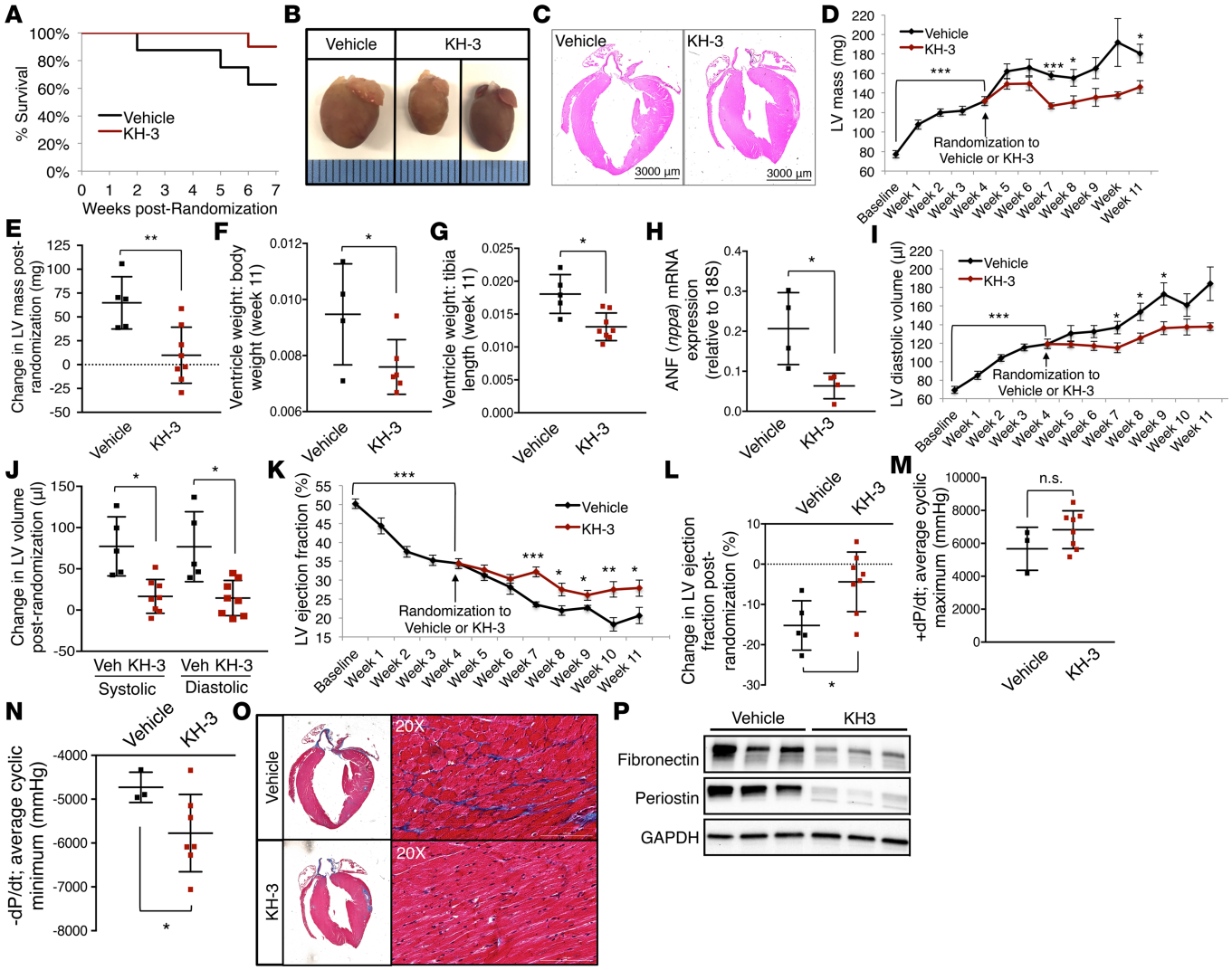

Figure 7. Pharmacological inhibition of HuR following the initial onset of pathological LVH reduces progression to heart failure. (**A**) Kaplan Meier survival curve of mice treated with KH-3 or vehicle after randomization (randomization occurred 4 weeks after TAC surgery). (**B**) Whole hearts isolated 11 weeks after TAC from mice treated with vehicle or KH-3. (**C**) H&E stains of heart sections from mice treated with vehicle or KH-3. Scale: 3000 μm. (**D**) LV mass determined by weekly echocardiogram from baseline to 11 weeks after TAC (with KH-3 or vehicle treatment beginning at 4 weeks after TAC). (**E**) Total change in LV mass of mice treated with KH-3 or vehicle from randomization (4 weeks after TAC) to 11 weeks after TAC. (**F**) Ventricular weight/body weight ratio and (**G**) ventricular weight/tibia length of mice treated with KH-3 or vehicle 11 weeks after TAC. (**H**) qPCR of ANF mRNA levels from cardiac tissue of mice treated with KH-3 or vehicle 11 weeks after TAC. (**I**) LV diastolic volume determined by weekly echocardiogram from baseline to 11 weeks after TAC (with KH-3 or vehicle treatment beginning 4 weeks after TAC). (**J**) Total change in left ventricular systolic and diastolic volume of mice treated with KH-3 or vehicle from randomization (4 weeks after TAC) to 11 weeks after TAC. (**K**) LV ejection fraction determined by weekly echocardiogram from baseline to 11 weeks after TAC (with KH-3 or vehicle treatment beginning 4 weeks after TAC). (**L**) Total change in LV ejection fraction of mice treated with KH-3 or vehicle from randomization (4 weeks after TAC) to 11 weeks after TAC. (**M**) Positive and (**N**) negative ventricular contractility (dP/dt) of KH-3– and vehicle-treated mice 11 weeks after TAC. (**O**) Masson's trichrome images of sectioned KH-3– and vehicle-treated hearts isolated 11 weeks after TAC. Scale bar: 100 μm. (**P**) Western blot of periostin and fibronectin (GAPDH loading control) in cardiac tissue isolated from mice treated with KH-3 or vehicle. Where appropriate, 2-way ANOVA and 2-tailed Student's *t* tests were performed. **P* <0.05, ***P* <0.01, and ****P* <0.001 for indicated comparisons. Data shown as means ± SEM. *n* ≥ 5 per group.

cardiomyocytes remain unclear. HuR has been shown to mediate TGF-β expression and profibrotic functions in fibroblasts, as well as macrophages (17, 21), and our data show that HuR may play a similar role in the myocytes, as HuR knockdown dramatically reduced NRVM expression of TGF-β in response to phenylephrine. Our data also show that *Tgfb* was a directly bound target of HuR and that HuR stabilized *Tgfb* mRNA. Moreover, a central role for HuR in controlling myocyte-mediated paracrine activation of fibrotic signaling would explain our RNA-seq results demonstrating that many of the HuR-dependent genes were identified as having profibrotic roles. Interestingly, *Tgfb* itself was

not among the genes that we found to be differentially regulated by TAC or HuR but is supported by seminal work by Villarreal and Dillman showing that *Tgfb* mRNA expression was increased early (within 12 hours) following aortic banding but returned to baseline within 2 weeks (22). At least a few of the genes identified as having changed in a HuR-dependent manner are not thought to be expressed by myocytes, which would suggest an indirect or much farther–upstream regulation by HuR (e.g., loss of HuR-dependent TGF-β expression in myocytes and a subsequent decrease in paracrine activation of myofibroblasts). However, 50 of the 59 HuR-dependent genes are predicted to have conserved HuR binding sites, representing a significant enrichment compared with predicted transcriptome-wide HuR binding sites (Fisher's exact Test, $P < 0.05$; Supplemental Table 5). On the other hand, in our data showing a colocalization of HuR activation and fibrosis, HuR appears to be activated in more cell types than myocytes. Therefore, future work will explore the role of HuR in additional cell types in the heart, as well — specifically myofibroblasts.

One of the more significant aspects of this work is that it establishes HuR inhibition as a potentially viable therapeutic approach to the clinical treatment of pathological LVH and HF. In demonstrating the efficacy of pharmacological targeting of HuR, we took a more clinically relevant approach of allowing the mice to progress out to 4 weeks after TAC when pathological LVH could already be observed prior to randomization to drug or vehicle. We show that a chronic (7 week) treatment with a small molecule inhibitor of HuR, following the initial development of a pathological LV hypertrophy, improved survival and stunted pathological progression of LVH, while eliciting no observable deleterious off-target effects to other tissues.

In summary, our results demonstrate that HuR activation in hypertrophic myocytes contributes to pathological LV remodeling in response to pressure overload. This is demonstrated through a preservation of LV function and inhibition of LV dilation following TAC in cardiac-specific HuR-deletion mice. Furthermore, we show that TGF-β expression and the development of cardiac fibrosis are inhibited in the absence of HuR, suggesting these pathways as a central mechanistic target of HuR activation in the myocyte. Finally, these results identify HuR as a potentially novel therapeutic target to prevent or reduce pathological progression of LVH in response to pressure overload.

Methods

Mouse models. HuR-floxed mice were described by Ghosh et al. (10) and obtained from The Jackson Laboratory (stock no. 021431). To generate a cardiac-specific inducible HuR-deletion model, HuR-floxed mice were crossed with mice expressing a cardiac myocyte–specific inducible Cre recombinase (*αMHC-mER-Cre-mER*) (The Jackson Laboratory, stock no. 005657) (11). HuR deletion was achieved through a daily i.p. injection of 4-hydroxy-tamoxifen (4-OHT; 60 mg/kg/day; Tocris Bioscience) for 5 days, as previously described (11). Mice were then allowed to recover for a minimum of 10 days following 4-OHT dosing prior to being incorporated into studies. Mice for KH-3 drug studies and RNA immunoprecipitation were WT C57Bl/6 mice obtained from The Jackson Laboratory (stock no. 000664). All mice were male and 10–16 weeks old at time of surgery. For tissue collection, tissues were removed and either flash frozen or fixed in 4% paraformaldehyde in PBS for further analysis.

Pharmacological HuR inhibition. HuR was pharmacologically inhibited using the small molecule KH-3, a second generation of HuR inhibitor compounds previously described by Wu et al. (23). For HuR inhibition, the KH-3 was i.p. injected 3× weekly at a dose of 60 mg/kg.

TAC. Pressure overload of the LV was induced by TAC surgery, as previously described (24, 25). Briefly, animals were anesthetized under isoflurane, intubated, and ventilated. Following sternotomy, a 7-0 silk suture was used to tie down the aorta (between the innominate and left carotid arteries) around a 27-gauge needle (which was subsequently removed) to produce a constriction of uniform and reproducible diameter. Sham-operated animals were subjected to the identical surgical procedures, besides the fact that the suture was not tied to produce an occlusion.

In vivo hemodynamic measurements. Pressure gradients across the aortic constriction site were determined in all animals by simultaneous pressure recording in the left and right carotid arteries, as previously described (24). As a terminal procedure, mice were weighed and anesthetized using an i.p. injection of ketamine (50 μg/g; Patterson Veterinary) and inactin (thiobutabarbital, 100 μg/g, MilliporeSigma). A 1.4-French Mikro-Tip Millar catheter pressure transducer was used to determine carotid pressure and subsequently advanced into the LV to determine dynamic pressure response and function, as previously described (26, 27). Following pressure recording, hearts were removed and atria were dissected away prior

to weighing and either fixing or flash freezing for further analysis.

Echocardiography. All echocardiographic studies were performed, as previously described (28). Briefly, mice were anesthetized with isoflurane (Patterson Veterinary), and body temperature was maintained at 37°C during imaging. Using a Vevo 2100, parasternal images were obtained in short and long axes in 2-dimensional mode and motion-mode (M-mode) for quantification. These were then analyzed using VevoStrain software (Vevo 2100, v1.1.1 B1455, Visualsonic). *iCM-HuR*$^{-/-}$ mice had baseline echocardiographic measurements before and after tamoxifen treatment, and all mice had measurements weekly following TAC until euthanasia.

NRVM isolation and culture. NRVMs were isolated using collagenase digestion and adhesion differential from fibroblasts. Sprague Dawley neonatal rats (1–2 days old) were decapitated, and the hearts were isolated. Following removal of the atria, the ventricles were cut into small pieces and digested first in 0.05% trypsin/EDTA (Corning) overnight and then in collagenase II (Thermo Fisher Scientific) for 30 minutes. Cells were then spun at 100 *g*, followed by a 40-minute preplating process on nontreated plates to allow the fibroblasts to adhere. The nonadherent NRVMs were then transferred to cell culture–treated dishes in MEMα media (Thermo Fisher Scientific) with 10% FBS.

Histological analysis. Fixed hearts were paraffin embedded and sectioned at 6-μm thickness by the CCHMC Department of Pathology Research Core and were subsequently stained with H&E and/or Masson's trichrome (MT). IF of HuR was performed on human and mouse failing heart samples. Samples were deparaffinized with xylene and rehydrated in serial ethanol dilutions. The samples were then heated in a sodium citrate solution (10 mM sodium citrate, 0.5% Tween20, pH 6) for 20 minutes for antigen retrieval. Triton-X 100 (0.06% solution) was used to permeabilize the samples for 30 minutes. The tissues were incubated in blocking solution (5% BSA, MilliporeSigma) for 1 hour, followed by primary HuR antibody (Abcam, ab200342) overnight and Alexa Fluor secondary antibody (Thermo Fisher Scientific, A11008) for 1 hour. For DAB staining, following antigen retrieval, samples were incubated in 1% hydrogen peroxide to block endogenous peroxidase activity, followed by blocking in 5% BSA. They were then incubated overnight in primary HuR antibody (Santa Cruz Biotechnology Inc., sc-5261), followed by HRP secondary antibody (Bio-Rad, 172-1011) for 1 hour and DAB substrate for 5 minutes. Images were taken using a BioTek Cytation 5.

Protein isolation and Western blotting. Total protein was isolated from crushed tissue in RIPA buffer with 0.5 mM DTT, 0.2 mM sodium-orthovanadate, and a protease inhibitor mixture tablet (Complete mini; Roche Applied Science). Protein extract (25 μg per lane) was separated on a 10% polyacrylamide gel and transferred to a nitrocellulose membrane. Blocking was performed for 1 hour at room temperature using 5% dry milk in 0.1% Tween 20, tris-buffered saline (T-TBS). Primary antibodies for periostin (Novus Biologicals, NBP1-30042), fibronectin (Abcam, ab2413), and GAPDH (Santa Cruz Biotechnology Inc., sc-25778) were incubated overnight at 4°C, and secondary antibodies were incubated for 1–2 hours at room temperature in T-TBS.

RNA isolation and quantitative PCR (qPCR). RNA was isolated using a Macherey-Nagel NucleoSpin RNA kit, and cDNA was synthesized using a BioScript All-in-One cDNA Synthesis SuperMix (BioTool). Samples were run on a Stratagene Mx3005P (Agilent Technologies) using ABsolute Blue SYBR Green ROX (Thermo Fisher Scientific) to assess levels of ANF, BNP, and 18S. Results were analyzed using the ΔΔCt method, normalized to 18S. Primers are as listed: ANF, F, 5′-AGGAGAAGATGCCGGTAG-3′, R, 5′-GCTTTTCAAGAGGGCAGA-3′; BNP, F, 5′-AAGTCCTAGCCAGTCTCCAGA-3′, R, 5′-GAGCTGTCTCTGGGCCATTTC-3′; 18S, F, 5′-AGTCCCTGCCCTTTGTACACA-3′, R, 5′-CCGAGGGCCTCACTAAACC-3′. TGF-β, F, 5′-CAATTCCTGGCGTTACCTTG-3′, R, 5′-CCCTGTATTCCGTCTCCTTG-3′; GAPDH, F, 5′-ACCACAGTCCATGCCATCAC-3′, R, 5′-TCCACCACCCTGTTGCTGTA-3′.

RNA immunoprecipitation. Protein G magnetic beads (Pierce, 88847) were washed 3 times with wash buffer (50 mM Tris, 150 mM NaCl, 1 mM $MgCl_2$, 0.05% NP-40). The beads were then incubated with either 2 μg HuR antibody (Abcam, ab28660) or a control secondary antibody, goat anti-rabbit (Invitrogen, 65-6120). Cardiac tissue from C57Bl/6 mice treated with either vehicle (DMSO), or HuR inhibitor (10 mg/kg DHTS; MilliporeSigma, D0947) was minced in PBS and triturated using the Bead Bug microtube homogenizer (Benchmark Scientific) to achieve a single cell suspension. The cells were then crosslinked using the Stratalinker UV crosslinker (400 μJ × 3). The cells were then spun down (4°C, 3000 rpm, 5 minutes), and the pellet was resuspended in lysis buffer (100 mM KCl, 5 mM $MgCl_2$, 10 mM Hepes, 0.5% NP-40, protease inhibitor

cocktail; Pierce) and lysed with a dounce homogenizer. The lysed cells were added to the prepared protein G beads and incubated for 1 hour at room temperature using a Hula Mixer (Invitrogen). After 1 hour, the cells were washed 5 times with lysis buffer. RNA was eluted using 100 μl of lysis buffer with 2.5 μl of Proteinase K (20 mg/ml) and incubating at 55°C for 30 minutes with mixing. RNA was purified using phenol/chloroform isolation and a Macherey-Nagel NucleoSpin RNA kit (as described above).

RNA stability. NRVMs were treated with 2 mM Actinomycin D (MilliporeSigma, A1410), DMSO vehicle, or Actinomycin D + HuR inhibitors CMLD1/2 (used previously in Slone et al.; ref. 8). RNA was collected at 0, 3, 8, and 24 hour time points and analyzed for *Tgfb* expression.

RNA-seq analyses. RNA was isolated as described in Slone et al. (8), and poly(A) library and sequencing were conducted at the DNA sequencing and Genotyping Core at the CCHMC. RNA was quantified with a Qubit 3.0 Flourometer (Invitrogen). Total RNA (150–300 ng) was poly(A) selected and converted to cDNA with a TruSeq Stranded mRNA Library Preparation Kit (Illumina). Different 8-base molecular barcodes were added to allow for high-level multiplexing. After 15 cycles of PCR amplification, libraries were sequences on a HiSeq 2500 sequencing system (Illumina) in Rapid Mode.

Sequenced reads were trimmed and filtered for quality with Trimmomatic, as previously described (29). Libraries were examined for quality at each step with the use of FastQC. Reads were mapped to the mouse genome (GRCm38) with the use of CLC Genomics Workbench (v. 9.5.1, Qiagen Co.). Each RNA-seq read was matched allowing 50% overlap at 95% matching to each transcript. The maximum number of mismatches allowed for each mapped read was set at 2. Gene expression was set as reads per kilobase million (RPKM). Data analyses were conducted through the use of CLC Genomics with the Advanced RNA-seq plugin (1.5). Statistical tests for assessment of differential expression were conducted with a negative binominal generalized linear model with edgeR (30) with a FDR of 0.01. PCA was based upon the normalized expression levels of each transcript with the use of the PCA package of R (version 3.3.2). GO of differential regulated transcripts was conducted with the use of g:Profiler (31). Complete lists of transcripts with differential expression in relation to TAC are provided in Supplemental Table 1. RNA-seq data has been deposited to NCBI Sequence Read Archive (https://www.ncbi.nlm.nih.gov/sra) and is available under the Bioproject PRJNA434656.

Prediction of HuR binding sites was done using RBPMap (http://rbpmap.technion.ac.il) (32). Statistical significance of enrichment of HuR binding sites was determined using a Fisher's exact test.

All chemicals and reagents were purchased from Thermo Fisher Scientific, unless otherwise noted.

Statistics. Statistical analysis was performed using GraphPad PRISM software. Primary statistical tests include 2-tailed Student's *t* test for single comparisons and 2-way or 2-way repeated-measures ANOVA for multiple comparisons. A *P* value of less than 0.05 was considered significant.

Study approval. All animal procedures were performed with the approval of the IACUC of the University of Cincinnati and in accordance with the NIH *Guide for the Care and Use of Laboratory Animals* (National Academies Press, 2011).

Author contributions

LCG and SRA contributed equally to the writing and preparation of this manuscript, as well as to the experimental design, execution, and data analysis. LCG performed all HuR IHC staining and Western blotting and contributed to experimental design, data collection, and analysis. SRA designed, executed, and oversaw the KH-3 in vivo experiments and provided general oversight and coordination of all animal experiments. SS performed all NRVM isolation, culture, and experiments. LL assisted with RNA isolation and qPCR experimental execution and analysis. MLN performed all TAC surgeries and in vivo pressure catheterizations. XW assisted with experimental design for KH-3 studies, as well as synthesis of KH-3. NR performed the weekly echocardiograms and echocardiography analysis. SMJ performed all H&E and Masson's trichome staining. APO assisted with experimental design for histological analyses. JA and SR were responsible for the synthesis of KH-3. BCB assisted with general experimental design and provided human cardiac tissue. JNL provided expertise with regard to experimental design, execution, and analysis of TAC and in vivo catheterization experiments. JBB provided all analysis and interpretation of RNA-seq results. LX assisted with experimental design for KH-3 studies and collaboratively provided KH-3 for use in this study. JR assisted with interpretation of echocardiography data. MT oversaw all experimental design, execution, analysis, interpretation, and communication of results. All authors contributed to the final editing and approval of the final version of this manuscript.

Acknowledgments

The authors would like to thank Min Jiang and Mariah Worley for their partial assistance with echocardiography measurements, as well as Charles Perkins and Logan Fulford for providing technical assistance with IHC. This work was funded in part by an American Heart Association Scientist Development grant SDG27360004 (to MT) and NIH grants R01 HL132111 (to MT) and R01 CA178831/CA191785 (to LX and JA). LCG was supported by NIH T32 HLHL125204.

Address correspondence to: Michael Tranter, 231 Albert Sabin Way, CVC 3936, Mail Location 0586, Cincinnati, Ohio 45267, USA. Phone: 513.558.2356; Email: michael.tranter@uc.edu.

1. Frey N, Katus HA, Olson EN, Hill JA. Hypertrophy of the heart: a new therapeutic target? *Circulation*. 2004;109(13):1580–1589.
2. Guyatt GH, Devereaux PJ. A review of heart failure treatment. *Mt Sinai J Med*. 2004;71(1):47–54.
3. Ferrario CM, Mullick AE. Renin angiotensin aldosterone inhibition in the treatment of cardiovascular disease. *Pharmacol Res*. 2017;125(Pt A):57–71.
4. Doller A, Pfeilschifter J, Eberhardt W. Signalling pathways regulating nucleo-cytoplasmic shuttling of the mRNA-binding protein HuR. *Cell Signal*. 2008;20(12):2165–2173.
5. Srikantan S, Gorospe M. HuR function in disease. *Front Biosci (Landmark Ed)*. 2012;17:189–205.
6. Suresh Babu S, Joladarashi D, Jeyabal P, Thandavarayan RA, Krishnamurthy P. RNA-stabilizing proteins as molecular targets in cardiovascular pathologies. *Trends Cardiovasc Med*. 2015;25(8):676–683.
7. Rajasingh J. The many facets of RNA-binding protein HuR. *Trends Cardiovasc Med*. 2015;25(8):684–686.
8. Slone S, et al. Activation of HuR downstream of p38 MAPK promotes cardiomyocyte hypertrophy. *Cell Signal*. 2016;28(11):1735–1741.
9. Doller A, et al. High-constitutive HuR phosphorylation at Ser 318 by PKC{delta} propagates tumor relevant functions in colon carcinoma cells. *Carcinogenesis*. 2011;32(5):676–685.
10. Ghosh M, et al. Essential role of the RNA-binding protein HuR in progenitor cell survival in mice. *J Clin Invest*. 2009;119(12):3530–3543.
11. Sohal DS, et al. Temporally regulated and tissue-specific gene manipulations in the adult and embryonic heart using a tamoxifen-inducible Cre protein. *Circ Res*. 2001;89(1):20–25.
12. van Berlo JH, Maillet M, Molkentin JD. Signaling effectors underlying pathologic growth and remodeling of the heart. *J Clin Invest*. 2013;123(1):37–45.
13. Travers JG, Kamal FA, Robbins J, Yutzey KE, Blaxall BC. Cardiac Fibrosis: The Fibroblast Awakens. *Circ Res*. 2016;118(6):1021–1040.
14. Hill JA, et al. Cardiac hypertrophy is not a required compensatory response to short-term pressure overload. *Circulation*. 2000;101(24):2863–2869.
15. Schiattarella GG, Hill TM, Hill JA. Is Load-Induced Ventricular Hypertrophy Ever Compensatory? *Circulation*. 2017;136(14):1273–1275.
16. Krishnamurthy P, Rajasingh J, Lambers E, Qin G, Losordo DW, Kishore R. IL-10 inhibits inflammation and attenuates left ventricular remodeling after myocardial infarction via activation of STAT3 and suppression of HuR. *Circ Res*. 2009;104(2):e9–18.
17. Krishnamurthy P, et al. Myocardial knockdown of mRNA-stabilizing protein HuR attenuates post-MI inflammatory response and left ventricular dysfunction in IL-10-null mice. *FASEB J*. 2010;24(7):2484–2494.
18. Bujak M, Frangogiannis NG. The role of TGF-beta signaling in myocardial infarction and cardiac remodeling. *Cardiovasc Res*. 2007;74(2):184–195.
19. Davis J, Molkentin JD. Myofibroblasts: trust your heart and let fate decide. *J Mol Cell Cardiol*. 2014;70:9–18.
20. Rosenkranz S. TGF-beta1 and angiotensin networking in cardiac remodeling. *Cardiovasc Res*. 2004;63(3):423–432.
21. Bai D, Gao Q, Li C, Ge L, Gao Y, Wang H. A conserved TGFβ1/HuR feedback circuit regulates the fibrogenic response in fibroblasts. *Cell Signal*. 2012;24(7):1426–1432.
22. Villarreal FJ, Dillmann WH. Cardiac hypertrophy-induced changes in mRNA levels for TGF-beta 1, fibronectin, and collagen. *Am J Physiol*. 1992;262(6 Pt 2):H1861–H1866.
23. Wu X, et al. Identification and validation of novel small molecule disruptors of HuR-mRNA interaction. *ACS Chem Biol*. 2015;10(6):1476–1484.
24. Wansapura AN, Lasko VM, Lingrel JB, Lorenz JN. Mice expressing ouabain-sensitive α1-Na,K-ATPase have increased susceptibility to pressure overload-induced cardiac hypertrophy. *Am J Physiol Heart Circ Physiol*. 2011;300(1):H347–H355.
25. Rindler TN, Lasko VM, Nieman ML, Okada M, Lorenz JN, Lingrel JB. Knockout of the Na,K-ATPase α2-isoform in cardiac myocytes delays pressure overload-induced cardiac dysfunction. *Am J Physiol Heart Circ Physiol*. 2013;304(8):H1147–H1158.
26. Lorenz JN. A practical guide to evaluating cardiovascular, renal, and pulmonary function in mice. *Am J Physiol Regul Integr Comp Physiol*. 2002;282(6):R1565–R1582.
27. Florea S, et al. Constitutive phosphorylation of inhibitor-1 at Ser67 and Thr75 depresses calcium cycling in cardiomyocytes and leads to remodeling upon aging. *Basic Res Cardiol*. 2012;107(5):279.
28. Koch SE, et al. Probenecid: novel use as a non-injurious positive inotrope acting via cardiac TRPV2 stimulation. *J Mol Cell Cardiol*. 2012;53(1):134–144.
29. Bolger AM, Lohse M, Usadel B. Trimmomatic: a flexible trimmer for Illumina sequence data. *Bioinformatics*. 2014;30(15):2114–2120.

30. Robinson MD, McCarthy DJ, Smyth GK. edgeR: a Bioconductor package for differential expression analysis of digital gene expression data. *Bioinformatics*. 2010;26(1):139–140.
31. Reimand J, et al. g:Profiler-a web server for functional interpretation of gene lists (2016 update). *Nucleic Acids Res*. 2016;44(W1):W83–W89.
32. Paz I, Kosti I, Ares M, Cline M, Mandel-Gutfreund Y. RBPmap: a web server for mapping binding sites of RNA-binding proteins. *Nucleic Acids Res*. 2014;42(Web Server issue):W361–W367.